Supporting information

Oxygen-induced defect-healing and photo-brightening of halide perovskite semiconductors: science and application

Like Huang[a, b] *, Ziyi Ge[a, c] *, Xiaoli Zhang[d], Yuejin Zhu[b]

[a]*Ningbo Institute of Materials Technology and Engineering (NIMTE), Chinese Academy of Sciences (CAS), Ningbo 315201, China. E-mail: huanglike@nbu.edu.cn*

[b]*Department of Microelectronic Science and Engineering, School of Physical Science and Technology, Ningbo University, Zhejiang 315211, China*

[c]*Center of Materials Science and Optoelectronics Engineering, University of Chinese Academy of Sciences, Beijing 100049, China*

[d]*School of Materials Science and Engineering, Zhengzhou University, Zhengzhou 450001, China. E-mail: geziyi@nimte.ac.cn*

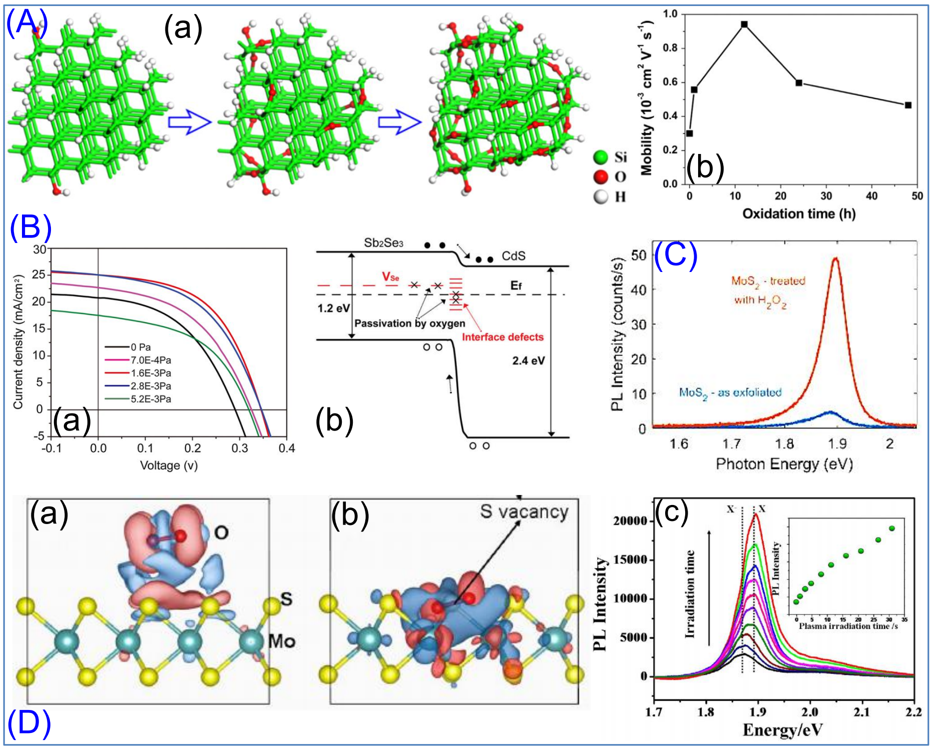

Fig. **S1** (A) Oxygen passivation of silicon NCs: (a) Possible surface passivation process during controlled oxidation and (b) Dependence of field effect carrier mobility on Si NC oxidation time. Reprinted with permission from Ref.[1]. Copyright 2014 Elsevier Ltd. (B) Oxygen passivation of Sb_2Se_3 solar cell: (a) *J-V* curves of the CdS/Sb_2Se_3 solar cells grown with oxygen partial pressures varying from 0 to 5.2×10^{-3} Pa and (b) Sketchy band diagram between Sb_2Se_3 and CdS without and with the addition of oxygen in the whole Sb_2Se_3 films deposition. Reprinted with permission from Ref.[2]. Copyright 2015 Wiley-VCH. (C) PL enhancement of monolayer MoS_2 before and after treatment with H_2O_2. Reprinted with permission from Ref.[3]. Copyright 2017 The Royal Society of Chemistry. (D) Oxygen bonding induced strong PL enhancement of MoS_2: charge density difference of O_2 molecule physisorbed on perfect monolayer MoS_2 (a) and chemisorbed on defective monolayer MoS_2 containing a mono-sulfur vacancy (b). PL spectra of monolayer MoS_2 after oxygen plasma irradiation with different durations (c). Reprinted with permission from Ref.[4]. Copyright 2014 American Chemical Society.

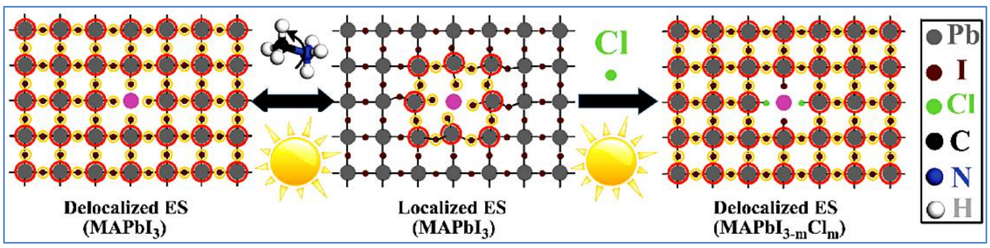

Fig. **S2** Schematic picture of the dynamic (MA orientation) and static (Cl doping) healing mechanisms. The crossover from spatially localized to delocalized excited states (ES) in defective perovskites is reflected by the extension of charge densities in the vicinity of the vacancies (shown in magenta color). The electron (hole) density is shown by red (yellow) circles on lead (iodine) ions. Reprinted with permission from Ref.[5]. Copyright 2018 Wiley-VCH.

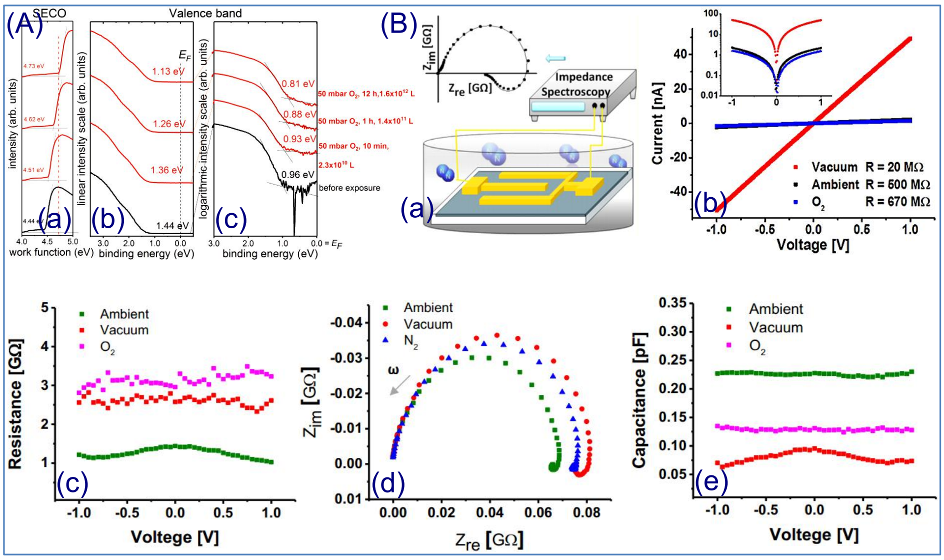

Fig. **S3** (A) UPS spectra of a $MAPbI_{3-x}Cl_x$ perovskite film before (black) and after (red) oxygen exposure to 50 mbar. (a) SECO and same valence band spectra displayed on (b) a linear and (c) a logarithmic intensity scale for valence band onset determination. Reprinted with permission from Ref.[6]. Copyright 2018 Wiley-VCH. (B) Electrochemical process of $MAPbI_{3-x}Cl_x$ under control environment (a) and the evolution of resistance (b, c) and capacitance values (d, e) of $MAPbI_{3-x}Cl_x$ film under different atmosphere. Reprinted with permission from Ref.[7]. Copyright 2016 American Chemical Society.

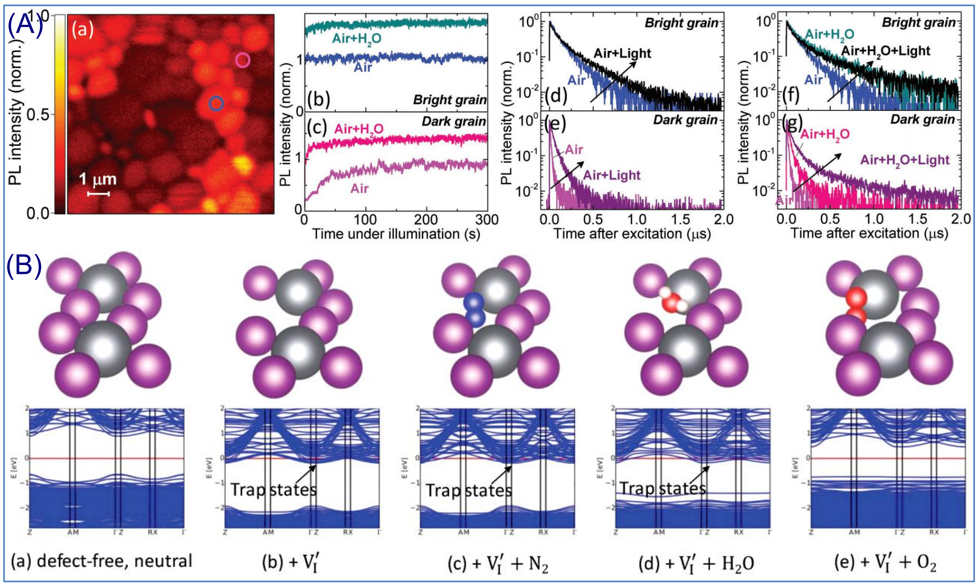

Fig. S4 Microscale PL properties in dry and humid air. (a) Confocal PL map of a $MAPbI_3$ film in dry air normalized to the maximum intensity. (b, c) Monitoring the emission (PL count rate) over time under illumination from: (b) a bright grain (blue circle in (a)) and (c) dark grain (pink circle in (a)) under dry air and under humidified (≈45% relative humidity) air. The PL intensity for each trace over time is given relative to the starting value for the bright grain in air, which is normalized to 1. (d, e) PL decays from the same (d) bright and (e) dark grains under dry air before and after the light soaking. (f, g) PL decays from the same bright (f) and dark (g) grains under dry air, humidified air, and after the light soaking in humidified air. (B) Surface atomic and electronic structures. Schematic representation of the local atomic-scale configurations of the surface termination layer (top row) and calculated band structures (bottom row) for the (110) surface of $MAPbI_3$. (a) Pristine uncharged surface, (b) negatively charged iodine vacancy into which the following molecules are adsorbed; (c) N_2, (d) H_2O, and (e) O_2. Reprinted with permission from Ref.[8]. Copyright 2018 Wiley-VCH.

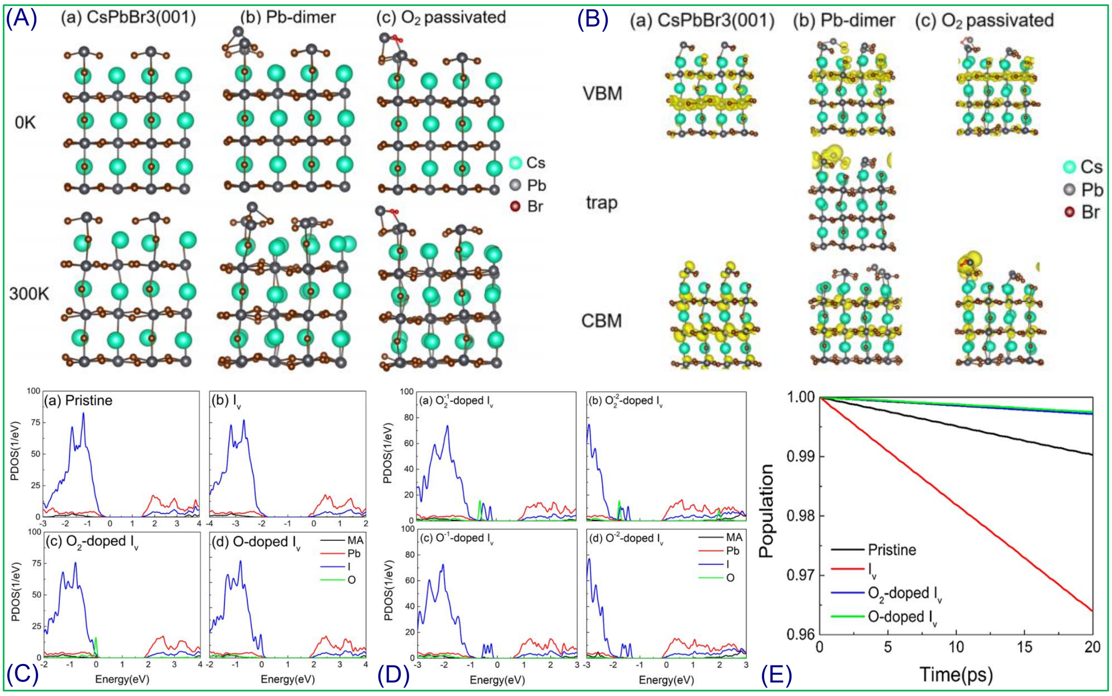

Fig. S5 (A) Simulated optimized geometry at 0 K (top panel) and a representative snapshot at 300 K of (a) pristine $CsPbBr_3$ (001) surface, (b) Pb-dimer, and (c) O_2 passivated Pb-dimer, respectively. (B) Charge densities obtained from a representative snapshot at 300 K for the key orbitals participating in charge trapping and recombination of (a) pristine $CsPbBr_3$ (001), (b) Pb-dimer, and (c) O_2 passivated systems. Reprinted with permission from Ref.[9]. Copyright 2019 American Chemical Society. (C) Projected density of states PDOS of (a) the pristine $MAPbI_3$ (001) surface, (b) Iv, (c) O_2-doped I_v, and (d) O-doped I_v systems. The Fermi level is set to zero. The superoxide level contributes to the system HOMO. (D) PDOS of the $MAPbI_3$ (001) system containing the I_v vacancy doped with charged oxygen species: (a) O^{1-} anion, (b) O^{2-} anion, (c) O_2^{1-} anion, and (d) O_2^{2-} anion. The Fermi level is set to zero. The corresponding nonradiative electron-hole recombination dynamics. Reprinted with permission from Ref.[10]. Copyright 2019 American Chemical Society.

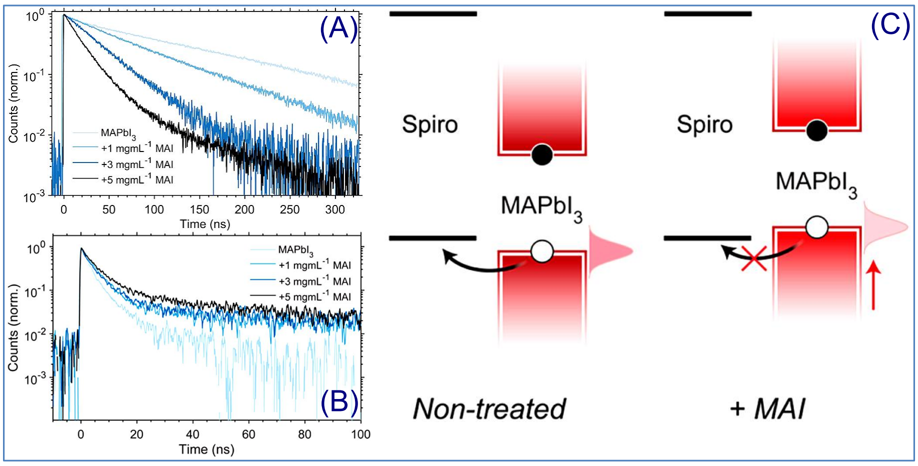

Fig. S6 TRPL for MAI-treated $MAPbI_3$ films without quencher layer (spiro-MeOTAD) (A) and with spiro-MeOTAD (B). Schematic of the VB alignment between spiro-MeOTAD and $MAPbI_3$ with and without MAI treatment (C). Reprinted with permission from Ref.[11]. Copyright 2019 American Chemical Society.

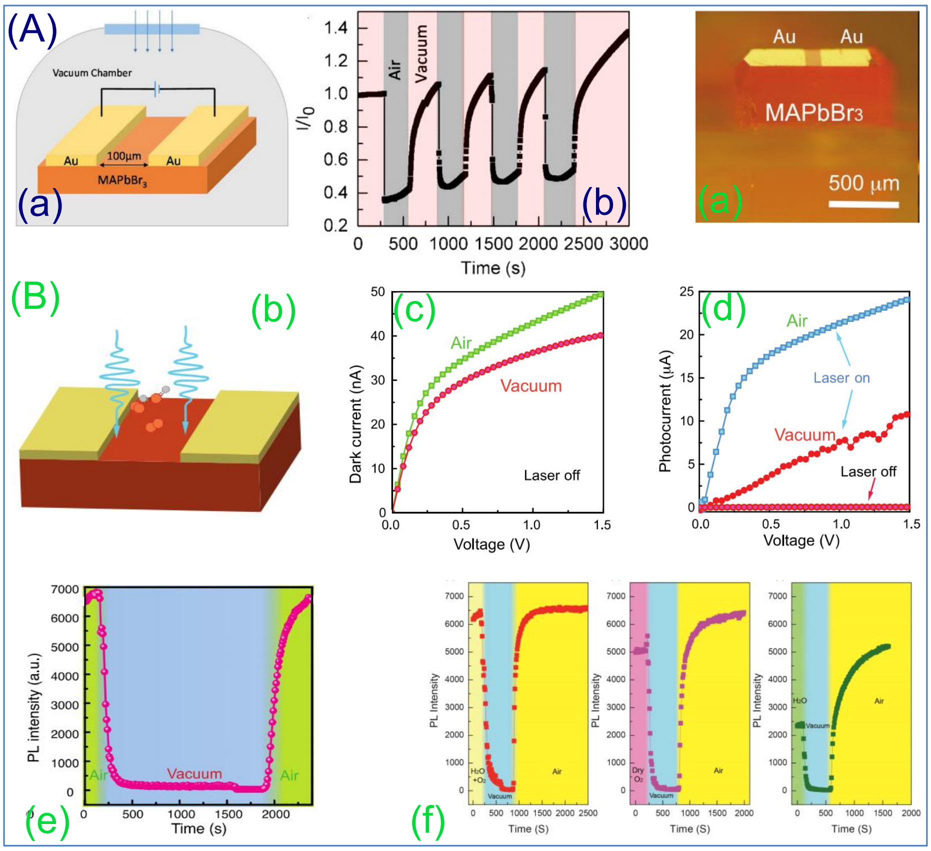

Fig. S7 A $MAPbBr_3$ SC with gold electrodes (a) and its photocurrents (b) measured under cyclical vacuum and atmosphere. Reprinted with permission from Ref.[12]. Copyright 2017 The Author(s). (B) Side-view (a) and structure (b) of a $MAPbBr_3$ SC device. *I-V* curves of the $MAPbBr_3$ SC device under dark (c) and under laser illumination (d) in air and vacuum. Variation in PL intensity of $MAPbBr_3$ SCs from air-vacuum-air environments (e). PL intensity variation in different gases (f).

Reprinted with permission from Ref.[13]. Copyright 2016 The Authors.

REFERENCE

1. Y. Ding, M. Sugaya, Q. Liu, S. Zhou, T. Nozaki, Oxygen passivation of silicon nanocrystals: Influences on trap states, electron mobility, and hybrid solar cell performance. Nano Energy **10**, 322-328 (2016).
2. X. Liu, C. Chen, L. Wang, J. Zhong, M. Luo, J. Chen, D.-J. Xue, D. Li, Y. Zhou, J. Tang, Improving the performance of Sb_2Se_3 thin film solar cells over 4% by controlled addition of oxygen during film deposition. Progress in Photovoltaics **23**, 1828-1836 (2015).
3. C. Schwermann, T. Stiehm, P. Tonndorf, R. Schneider, N. Doltsinis, Incorporation of oxygen atoms as a mechanism for photoluminescence enhancement of chemically treated MoS_2. Physical Chemistry Chemical Physics **20** (2018).
4. H. Nan, Z. Wang, W. Wang, Z. Liang, Y. Lu, Q. Chen, D. He, P. Tan, F. Miao, X. Wang, Strong photoluminescence enhancement of MoS_2 through defect engineering and oxygen bonding. ACS Nano **8**, 5738-5745 (2014).
5. G. Nan, X. Zhang, M. Abdi-Jalebi, Z. Andaji-Garmaroudi, S.D. Stranks, G. Lu, D. Beljonne, How methylammonium cations and chlorine dopants heal defects in lead iodide perovskites. Advanced Energy Materials, **8**, 1702754.1-1702754.9 (2018).
6. M. Ralaiarisoa, I. Salzmann, F.h. Zu, Effect of water, oxygen, and air exposure on $CH_3NH_3PbI_{3-x}Cl_x$ perovskite surface electronic properties. Advanced Electronic Materials **4** (2018).
7. A. Zohar, N. Kedem, I. Levine, D. Zohar, D. Cahen, Impedance spectroscopic indication for solid state electrochemical reaction in $CH_3NH_3PbI_3$ films. Journal of Physical Chemistry Letters **7**, 191-197 (2015).
8. R. Brenes, C. Eames, V. Bulović, M.S. Islam, S. Stranks, The impact of atmosphere on the local luminescence properties of metal halide perovskite grains. Advanced Materials **30**, 1706208 (2018).
9. L. Qiao, R. Long, Surface Pb-dimer passivated by molecule oxygen notably suppresses charge recombination in $CsPbBr_3$ Perovskites: Time-domain *ab initio* analysis. Journal of Physical Chemistry Letters **10**, 5499-5506 (2019).
10. J. He, W.-H. Fang, R. Long, O.V. Prezhdo, Superoxide/peroxide chemistry extends charge carriers' lifetime but undermines chemical stability of $CH_3NH_3PbI_3$ exposed to oxygen: Time-domain ab initio analysis. Journal of the American Chemical Society **141**, 5798-5807 (2019).
11. D. Meggiolaro, E. Mosconi, A. H. Proppe, R. Quintero-Bermudez, S. O. Kelley, E. H. Sargent, F. De Angelis, Energy level tuning at the $MAPbI_3$ perovskite/contact interface using chemical treatment. ACS Energy Letters **4**,

2181-2184 (2019).
12. H. Zhang, Y. Liu, H. Lu, W. Deng, K. Yang, Reversible air-induced optical and electrical modulation of methylammonium lead bromide ($MAPbBr_3$) single crystals. Appl. Phys. Lett. **111**, 103904.1-103904.5 (2017).
13. H.H. Fang, S. Adjokatse, H. Wei, J. Yang, G.R. Blake, J. Huang, J. Even, M.A. Loi, Ultrahigh sensitivity of methylammonium lead tribromide perovskite single crystals to environmental gases. Science Advances **2**, 1600534 (2016).